Downloaded from jnm.snmjournals.org by on March 15, 2017. For personal use only.

Longitudinal Amyloid Imaging in Mouse Brain with ^{11}C-PIB: Comparison of APP23, Tg2576, and APP$_{swe}$-PS1$_{dE9}$ Mouse Models of Alzheimer Disease

Anniina Snellman[1], Francisco R. López-Picón[1], Johanna Rokka[2], Mario Salmona[3], Gianluigi Forloni[3], Mika Scheinin[4], Olof Solin[2,5], Juha O. Rinne[6], and Merja Haaparanta-Solin[1]

[1]MediCity/PET Preclinical Laboratory, University of Turku, Turku PET Centre, Turku, Finland; [2]Radiopharmaceutical Chemistry Laboratory, University of Turku, Turku PET Centre, Turku, Finland; [3]Mario Negri Institute for Pharmacological Research, Milan, Italy; [4]Department of Pharmacology, Drug Development, and Therapeutics, University of Turku, and Unit of Clinical Pharmacology, Turku University Hospital, Turku, Finland; [5]Accelerator Laboratory, Åbo Akademi University, Turku PET Centre, Turku, Finland; and [6]Turku PET Centre, University of Turku, Turku University Hospital, Turku, Finland

Follow-up of β-amyloid (Aβ) deposition in transgenic mouse models of Alzheimer disease (AD) would be a valuable translational tool in the preclinical evaluation of potential antiamyloid therapies. This study aimed to evaluate the ability of the clinically used PET tracer ^{11}C-Pittsburgh compound B (^{11}C-PIB) to detect changes over time in Aβ deposition in the brains of living mice representing the APP23, Tg2576, and APP$_{swe}$-PS1$_{dE9}$ transgenic mouse models of AD. **Methods:** Mice from each transgenic strain were imaged with 60-min dynamic PET scans at 7−9, 12, 15, and 18−22 mo of age. Regional ^{11}C-PIB retention was quantitated as distribution volume ratios using Logan graphical analysis with cerebellar reference input, as radioactivity uptake ratios between the frontal cortex (FC) and the cerebellum (CB) during the 60-min scan, and as bound-to-free ratios in the late washout phase (40−60 min). Ex vivo autoradiography experiments were performed after the final imaging session to validate ^{11}C-PIB binding to Aβ deposits. Additionally, the presence of Aβ deposits was evaluated in vitro using staining with thioflavin-S and Aβ$_{1–40}$, Aβ$_{1–16}$, and Aβ$_{N3(pE)}$ immunohistochemistry. **Results:** Neocortical ^{11}C-PIB retention was markedly increased in old APP23 mice with large thioflavin-S–positive Aβ deposits. At 12 mo, the Logan distribution volume ratio for the FC was 1.03 and 0.93 (n = 2), increasing to 1.38 ± 0.03 (n = 3) and 1.34 (n = 1) at 18 and 21 mo of age, respectively. An increase was also observed in bound-to-free ratios for the FC between young (7- to 12-mo-old) and old (15- to 22-mo-old) APP23 mice. Binding of ^{11}C-PIB to Aβ-rich cortical regions was also evident in ex vivo autoradiograms of APP23 brain sections. In contrast, no increases in ^{11}C-PIB retention were observed in aging Tg2576 or APP$_{swe}$-PS1$_{dE9}$ mice in vivo, although in the latter, extensive Aβ deposition was already observed at 9 mo of age with immunohistochemistry. **Conclusion:** The results suggest that ^{11}C-PIB binding to Aβ deposits in transgenic mouse brain is highly dependent on the AD model and the structure of its Aβ plaques. Longitudinal in vivo ^{11}C-PIB uptake studies are possible in APP23 mice.

Key Words: Alzheimer disease; amyloid imaging; positron emission tomography; ^{11}C-PIB, Pittsburgh compound B

J Nucl Med 2013; 54:1434–1441
DOI: 10.2967/jnumed.112.110163

Received Dec. 17, 2012; revision accepted Mar. 14, 2013.
For correspondence or reprints contact: Anniina Snellman, Tykistökatu 6A, FI-20520 Turku, Finland.
E-mail: aepakk@utu.fi
Published online Jul. 5, 2013.
COPYRIGHT © 2013 by the Society of Nuclear Medicine and Molecular Imaging, Inc.

Many of the pathologic characteristics of Alzheimer disease (AD), including β-amyloid (Aβ) deposition, neuroinflammation, and changes in different neurotransmitter systems and glucose metabolism, can now be investigated with PET in living human subjects. PET provides a means to investigate the underlying pathologic processes, to make early and accurate diagnoses, and to evaluate the efficacy of novel AD treatments (*1,2*). ^{11}C-labeled Pittsburgh compound B (^{11}C-PIB) is the most commonly used PET tracer in studies on AD and enables the in vivo detection of Aβ deposits in the human brain (*3*). ^{11}C-PIB is a derivative of thioflavin-T with specific high-affinity binding to fibrillar Aβ (*4,5*).

Several transgenic mouse lines that overexpress specific genes, such as mutant forms of human amyloid precursor protein (APP) and presenilin 1 (PS1), that are known to cause familial AD have been developed for research purposes (*6*). These mice express many features of AD, including Aβ deposition, neuritic plaques, cerebral amyloid angiopathy, synaptic defects, gliosis, and signs of neurodegeneration and memory impairment (*7*). However, none of the current transgenic mouse models fully replicates the human disease: neurofibrillary tangles are absent, and little or no neuronal loss has been observed (*7,8*).

With PET tracers such as ^{11}C-PIB and scanners designed for small-animal PET imaging, longitudinal follow-up of Aβ deposition in transgenic mouse models of AD would have translational value in preclinical studies evaluating new therapeutic antiamyloid interventions and progression of amyloid pathology in mouse brain. However, attempts to perform in vivo small-animal ^{11}C-PIB PET imaging of the Aβ pathology in transgenic mouse models have yielded variable results (*9–12*). In earlier reports using APP-PS1 and Tg2576 mice, the specific binding of ^{11}C-PIB to transgenic mouse brain with abundant Aβ pathology was low, even at 12 and 22 mo of age (*9,10*). Because of the proposed paucity of high-affinity binding sites for ^{11}C-PIB in murine Aβ deposits, the specific radioactivity (SA) of the tracer has been suggested to be of importance, and increasing Aβ accumulation in APP23 mice has been successfully monitored in a preclinical in vivo PET study using ^{11}C-PIB with very high SA (290 ± 10 GBq/μmol at the end of synthesis) (*11*).

This study aimed to evaluate the ability of ^{11}C-PIB to detect changes over time in Aβ deposition in the brains of APP23,

Downloaded from jnm.snmjournals.org by on March 15, 2017. For personal use only.

Tg2576, and APP_{swe}-$PS1_{dE9}$ transgenic mouse models of AD. Because of the discrepancies observed in previous studies, we wanted to investigate the importance of the used mouse model for PIB-positive results by evaluating individual transgenic animals from the various AD strains in a longitudinal fashion, using the same imaging protocol, animal PET/CT device, and radiochemical production protocol of ^{11}C-PIB.

MATERIALS AND METHODS

Tracer Synthesis

^{11}C-PIB was synthesized at the Radiopharmaceutical Chemistry Laboratory of Turku PET Centre. Briefly, desmethyl-PIB was labeled with ^{11}C-methyltriflate, produced from ^{11}C-carbon dioxide, to obtain ^{11}C-PIB (*13*). ^{11}C-PIB was formulated for injection in physiologic propylene glycol/ethanol/0.1 M phosphate buffer (2:1:14, v:v:v). The mean SA of ^{11}C-PIB was 100 ± 27 GBq/μmol (mean ± SD of 45 batches) at the end of synthesis. The radiochemical purity exceeded 95% in all syntheses.

Animals

The study was approved by the Animal Experiment Board of the Province of Southern Finland. PET imaging was performed on female transgenic mice from the APP23 (n = 5, one male mouse included), Tg2576 (n = 4), and APP_{swe}-$PS1_{dE9}$ (n = 5) transgenic mouse lines, and female wild-type controls (n = 3, n = 3, n = 3, respectively). All 3 transgenic mouse lines express APP with the Swedish double-mutation K670 L and M671 L (APP_{swe}), which facilitates cleavage of APP near the β-secretase site and increases production of Aβ peptide.

APP23 mice (Novartis Pharma) express human $APP751_{swe}$ driven by the neuron-specific mouse Thy-1.2 gene fragment as promoter. Aβ immunoreactive plaques develop progressively in the neocortex and hippocampus and are associated with dystrophic neurites and gliosis (*14,15*). Tg2576 mice (B6;SJL-Tg(APPSWE)2576Kha; Taconic Farms Inc.) overexpress a 695-amino-acid form of human APP_{swe} controlled by the hamster prion protein promoter and develop Aβ plaques in the brain by the age of 9–10 mo (*16*). APP_{swe}-$PS1_{dE9}$ mice (Tg(APPswe, PSEN1DE9)85Dbo/J; Jackson Laboratories) overexpress a chimeric form of mouse–human $APP695_{swe,}$ and an exon-9–deleted variant of human PS1, both controlled by independent mouse prion protein promoter elements. Because of the coexpression of mutant APP and PS1, Aβ deposition is accelerated and starts by 6–7 mo of age (*17*). All animals were group-housed under standard conditions (temperature, 21°C ± 3°C; humidity, 55% ± 15%; lights on from 6:00 AM until 6:00 PM) and had ad libitum access to soy-free chow (RM3 (E) soya-free, 801710; Special Diets Service) and tap water. Soy-free chow was provided to prevent excess weight gain.

PET Imaging

APP23 and Tg2576 mice were imaged at 7−9, 12, 15, 18–19, and 21−22 mo of age. APP_{swe}-$PS1_{dE9}$ mice were evaluated only at 9, 12, 15, and 19 mo of age because of faster Aβ deposition in the brain. Wild-type mice were imaged at 12, 15, 19, or 27 mo of age. One to four animals from each strain were imaged at each time point. All mice were anesthetized with 2.5% isoflurane and kept warm with a heating pad and a bubble-wrap cover. The eyes were protected from drying with ophthalmic gel (Oftagel, 25 mg/g; Santen Oy). All PET scans were performed using an Inveon multimodality PET/CT device (Siemens Medical Solutions). After transmission scans were obtained for attenuation correction using the CT modality, 60-min dynamic PET scans in 3-dimensional list mode were started immediately following intravenous bolus injection of ^{11}C-PIB (injected dose, 8.7 ± 1.4 MBq; injected mass, 68 ± 23 ng; SA, 50 ± 15 GBq/μmol at the time of injection). The injected mass was minimized in order not to saturate the high-affinity ^{11}C-PIB binding sites in the brain. Time frames used for dynamic PET imaging were 30 × 10, 15 × 60, 4 × 300, and 2 × 600 s. Images were reconstructed using a 2-dimensional filtered backprojection algorithm, resulting in a voxel size of 0.78 × 0.78 × 0.80 mm, or approximately 0.5 mm^3. For image analysis, dynamic PET images were coregistered with the corresponding CT images, and volumes of interest (VOIs) were manually drawn on the entire brain (450 ± 53 mm^3), frontal cortex (FC, 46 ± 16 mm^3), neocortex (NC, 130 ± 20 mm^3), pons (8 ± 3 mm^3), and cerebellar cortex (CB, 12 ± 4 mm^3) with Inveon Research Workplace 3.0 (Siemens Medical Solutions) using the CT template and a stereotactic mouse brain atlas as anatomic reference (*18*). To minimize bias, VOIs were drawn on top of the coregistered CT image and were not guided by observed radioactivity in the brain. No differences were observed between the VOIs of the transgenic mice and wild-type controls ($P >$ 0.05 for all VOIs, unpaired t tests).

Analysis of PET Data

From the obtained time–activity curves, VOI/CB ratios were calculated for each frame of the dynamic data, and the regional retention of ^{11}C-PIB in the brain was quantitated using the graphical method developed by Logan et al. (*19*). Logan plots with input obtained from the cerebellar reference region were used to calculate distribution volume ratios (DVRs). Fit time was set from 5 to 60 min. In addition, bound-to-free ($B/F_{40–60}$) ratios for the late washout phase (40−60 min) were calculated from areas under the curve as (region − CB)/CB ratios. In APP_{swe}-$PS1_{dE9}$ mice, Aβ deposition was observed also in the CB at older ages. To verify the binding results in this mouse model, $B/F_{40–60}$ and VOI/CB ratios were also calculated using the pons as a secondary reference tissue.

Ex Vivo Digital Autoradiography

After the final PET scans at 21 (APP23), 22 (Tg2576), or 19 mo of age (APP_{swe}-$PS1_{dE9}$), retention of ^{11}C-PIB in the transgenic mouse brain was also evaluated with ex vivo autoradiography. For wild-type mice, ex vivo autoradiography studies were done at 22, 22, and 19 mo, respectively. The mice received an intravenous bolus injection of ^{11}C-PIB (10.2 ± 1.4 MBq) and were sacrificed with cardiac puncture under deep isoflurane anesthesia 10 min later. Brains were dissected and weighed, measured for ^{11}C-radioactivity with a γ-counter, and immediately frozen with isopentane chilled with dry ice. Coronal brain cryosections (20 μm) from the FC (approximately 2 mm from the bregma) and CB (approximately −7 mm from the bregma) were prepared on microscope slides, air dried, and apposed to an imaging plate (BAS-TR2025; Fuji Photo Film Co.) for approximately 1 h. The imaging plates were scanned with the BAS-5000 analyzer (Fuji) at a resolution of 25 × 25 μm. All analyses were performed using a computerized image analysis program (Aida 4.19; Raytest Isotopenmessgeräte, GmbH). Regions of interest were drawn on 8 sections from each brain, plate background was subtracted, and the images were analyzed for count densities, expressed as photostimulated luminescence per square millimeter.

Thioflavin-S and Immunohistochemical Analysis

Mice were sacrificed at various ages from 9 to 22 mo to obtain supporting data regarding Aβ deposition in the brain. Brain sections were stained with thioflavin-S (Sigma Aldrich) and anti-$Aβ_{1–16}$ antibody (6E10; Covance Inc.) as previously described (*20*). In addition, anti-$Aβ_{1–40}$ (Millipore) and anti-$Aβ_{N3(pE)}$ (ABIN459385; antibodies-online GmbH) primary antibodies were used for immunohistochemistry.

All staining was performed using thawed fresh-frozen sections postfixed in 4% paraformaldehyde. For $Aβ_{N3(pE)}$ and $Aβ_{1–40}$, sections were pretreated with 88% formic acid for 10 min. All sections were incubated in blocking solution for 30 min before staining with primary

Downloaded from jnm.snmjournals.org by on March 15, 2017. For personal use only.

TABLE 1
Differences in ^{11}C-PIB Binding and Aβ Pathology Between APP23, Tg2576, and APP$_{swe}$-PS1$_{dE9}$ Mice

	APP23 (n = 5)			Tg2576 (n = 4)			APP-PS1 (n = 5)		
Parameter	12 mo	18 mo	21 mo	12 mo	15 mo	22 mo	9 mo	13 mo	19 mo
FC/CB	—	↑	↑	—	—	—	—	—	—
Logan DVR	—	↑	↑	—	—	—	—	—	—
B/F$_{40–60}$	—	↑	↑	—	—	—	—	—	—
Thioflavin-S	*	**	***	—	*	*	*	**	**
Aβ$_{1–40}$	*	***	***	—	*	*	**	**	***
Aβ$_{N3(pE)}$	—	*	*	—	—	—	—	—	—

↑ = increase; — = no increase/no deposition; * = mild (0.5%−2%); ** = moderate (2%−10%); *** = extensive (>10%).

antibodies (dilution in blocking solution: anti-Aβ$_{N3(pE)}$, 1:400; Aβ$_{1–40}$, 1:300) for 48 h at 4°C in a humidified chamber. After washing, the sections were incubated with either a fluorescent secondary antibody (Alexa Fluor 568, 1:500; Invitrogen) and 4′,6-diamidino-2-phenylindole in blocking solution for 60 min at room temperature or a biotin-conjugated secondary antibody (1:400; Jackson Immuno Research Laboratories, Inc.) for 60 min, and with avidin-peroxidase conjugate (Vectastain ABC Kit; Vector Laboratories) for 60 min, before the staining was visualized using 3,3-diaminobenzidine tetrahydrochloride. Immunoreactivity was examined with a DMR microscope (Leica) under fluorescence filters or transmitted light. Pictures were captured using a U-TV1 X digital camera (Olympus Optical).

Quantitation of Aβ Deposition in the Brain

To further estimate the amount of thioflavin-S–stained and Aβ$_{1–40}$-immunoreactive deposits in the brain, microscope images were obtained from 5 different locations within the FC with ×10 magnification. Images were transformed to 8-bit black-and-white format using ImageJ 1.43u software. The threshold was set by comparison to the original images because of differences in background staining in different sections. The amount of Aβ deposition was calculated as the percentage stained area of the entire image area. Mean values of the 5 analyzed images were calculated for each mouse, and the amount of Aβ deposition was presented as this average fractional thioflavin-S–stained or Aβ$_{1–40}$-immunopositive area.

Data Analysis and Statistics

The results are reported as means ± SD ($n \geq 3$) or as individual values ($n < 3$). All statistical analysis was performed using the GraphPad Prism program (version 5.01; GraphPad Software). Differences in VOIs between the groups of all transgenic and wild-type mice were tested using unpaired t tests. Differences were considered statistically significant if the P value was less than 0.05.

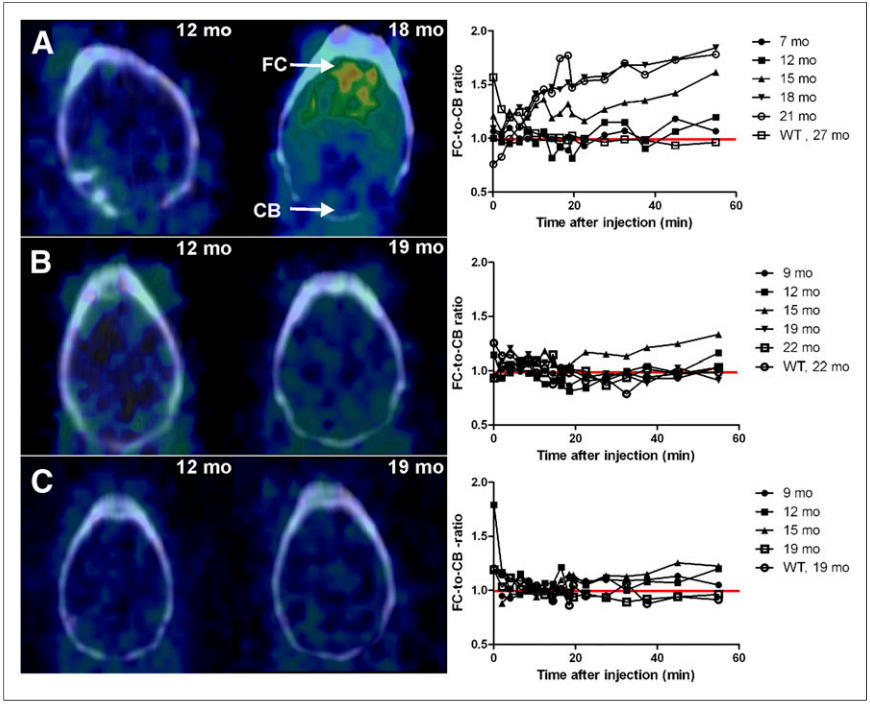


FIGURE 1. APP23 (A), Tg2576 (B), and APP$_{swe}$-PS1$_{dE9}$ (C) mice 12 mo and 18–19 mo old were imaged with small-animal ^{11}C-PIB PET/CT. Mean FC/CB ratios were calculated for every mouse line for the entire 60-min PET scan. PET images are summed at 35–60 min after injection. CB = cerebellum; FC = frontal cortex; WT = wild-type.

RESULTS

Differences in ^{11}C-PIB retention, development of Aβ pathology, and structure of Aβ deposits among the 3 different mouse models of AD are summarized in Table 1.

Follow-up of Aβ Deposition with ^{11}C-PIB PET

At 12 mo old, APP23 mice did not exhibit ^{11}C-PIB retention in the brain during 60-min PET scans, but at 18 mo, a clear increase in ^{11}C-PIB retention was observed in the PET images (Fig. 1A). In older APP23 mice, the FC/CB ratio started to increase approximately 10 min after injection, indicating tracer retention in the regions of increased Aβ deposition. The FC/CB ratio during the last imaging frame (50−60 min) was 1.62 at 15 mo of age (n = 1), 1.84 ± 0.36 at 18 mo (n = 3), and 1.78 at 21 mo (n = 1) (Fig. 1A). Wild-type mice as old as 27 mo demonstrated no increase in their FC/CB ratio during the 60-min scan. No ^{11}C-PIB retention in the brain or clear increase in FC/CB ratio was observed at any of the evaluated time points in Tg2576 mice (Fig. 1B) or APP$_{swe}$-PS1$_{dE9}$ mice (Fig. 1C), indicating little or no binding

Downloaded from jnm.snmjournals.org by on March 15, 2017. For personal use only.

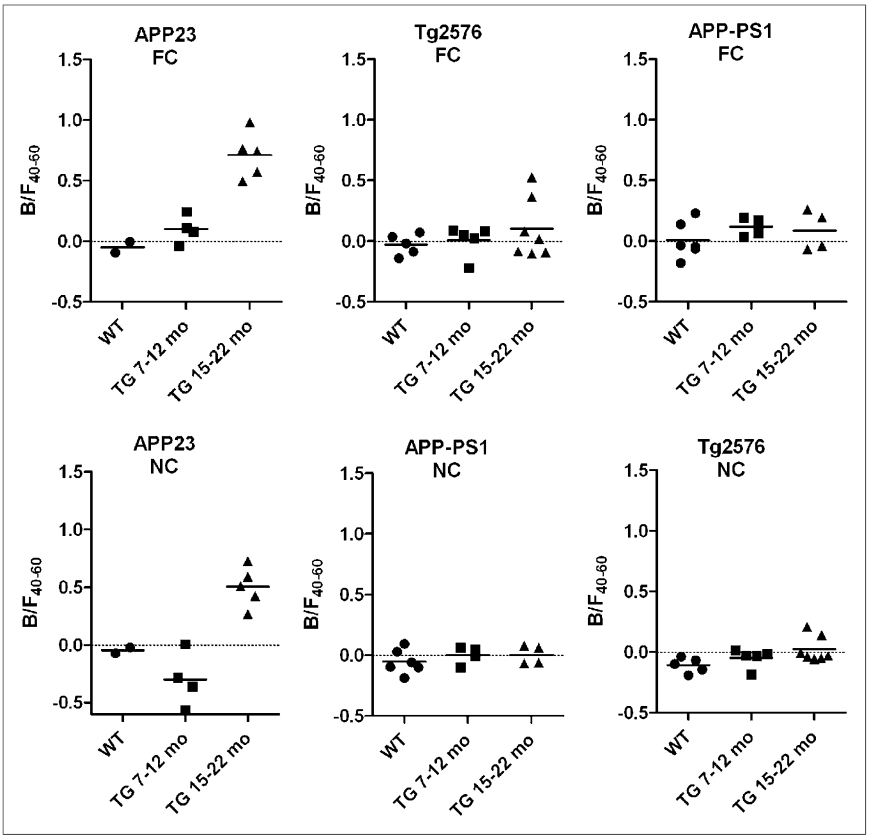


FIGURE 2. Bound-to-free (B/F) ratios were calculated at 40−60 min after injection for frontal cortex (FC) and neocortex (NC) of APP23, Tg2576, and APP_{swe}-$PS1_{dE9}$ mice imaged with in vivo PET at various time points. CB was used as reference region. WT = wild-type.

of ^{11}C-PIB in the brain. In APP_{swe}-$PS1_{dE9}$ mice, FC/pons ratio results were virtually identical to FC/CB results.

$B/F_{40–60}$ ratios were consistent with the FC/CB ratios, demonstrating an increase in aging APP23 mice but not in Tg2576 or APP_{swe}-$PS1_{dE9}$ mice. An increase in $B/F_{40–60}$ ratios for FC and NC were detected between young and old APP23 mice but not between young and old Tg2576 or APP_{swe}-$PS1_{dE9}$ mice (Fig. 2).

Quantitation of the imaging data using Logan graphical analysis with CB input provided consistent results with the FC/CB and $B/F_{40–60}$ ratios (Fig. 3). In APP23 mice, the Logan DVRs for FC showed no increase from 1.07 and 0.97 at 7 mo (n = 2) to 1.03 and 0.93 at 12 mo (n = 2). DVR was 1.19 at 15 mo (n = 1), increasing to 1.38 ± 0.03 at 18 mo (n = 3). No further increase was observed at 21 mo (DVR = 1.34, n = 1). For Tg2576 mice, Logan DVRs for the FC were 0.97 ± 0.06 at 9 mo (n = 3), 0.98 and 0.92 at 12 mo (n = 2), and 1.08 and 1.03 at 19 mo (n = 2). Even at 22 mo, the DVRs of Tg2576 mice were 1.10 and 0.93 (n = 2), resembling the DVRs of older wild-type mice (1.04 and 1.03, n = 2). No increases in Logan DVRs were observed in the APP_{swe}-$PS1_{dE9}$ mice. The DVRs for the transgenic mice were 1.07 and 0.99 at 9 mo, 1.04 and 1.09 at 12 mo, 0.98 and 1.03 at 15 mo, and 0.96 and 1.00 in the final evaluation at 19 mo (n = 2 for each set of measurements). Representative images from the Logan plots obtained to determine DVRs from the analyzed brain regions are shown in Supplemental Figure 1 (supplemental materials are available online at http://jnm.snmjournals.org).

Ex Vivo Autoradiography

Representative digital autoradiography images from sections of the FC are presented for APP23, Tg2576, APP_{swe}-$PS1_{dE9}$, and wild-type mice (Fig. 4A). Autoradiograms from the FC of an APP23 mouse clearly depict an increase in ^{11}C-PIB binding. The count density was higher in the FC than in the CB, and higher radioactivity colocalized with thioflavin-S–positive deposits. In Tg2576 and APP_{swe}-$PS1_{dE9}$ brain sections, the count density was higher in CB than FC because of nonspecific binding to cerebellar white matter (Fig. 4B). FC/CB ratios calculated from the autoradiograms were 1.62, 0.78, and 0.82 for transgenic APP23, Tg2576, and APP_{swe}-$PS1_{dE9}$ mice, respectively. Autoradiography images from CB are presented in Supplemental Figure 2.

Aβ Deposition in the Brain

Representative cortical images of thioflavin-S–positive deposits are presented in Figure 5A. Although APP23 mice exhibited only a few sparse fibrillar Aβ deposits at 12 mo, extensive amounts of large, thioflavin-S–positive, dense-cored deposits were observed at 18 and 21 mo in cortical regions. Hippocampal thioflavin-S staining was less prominent. The CB exhibited no Aβ deposits, even at 21 mo of age (Supplemental Fig. 3). Sparse thioflavin-S–positive Aβ deposits were first observed in Tg2576 mice at 15 mo. Even at 22 mo, the amount of deposition was low, and the deposits were small. Deposits were absent from the CB (Supplemental Fig. 3). APP_{swe}-$PS1_{dE9}$ mice exhibited thioflavin-S–positive deposits at 9 mo throughout the NC and in the hippocampus. Plaque load increased slightly as the mice aged; at 19 mo, deposits were already observed throughout the

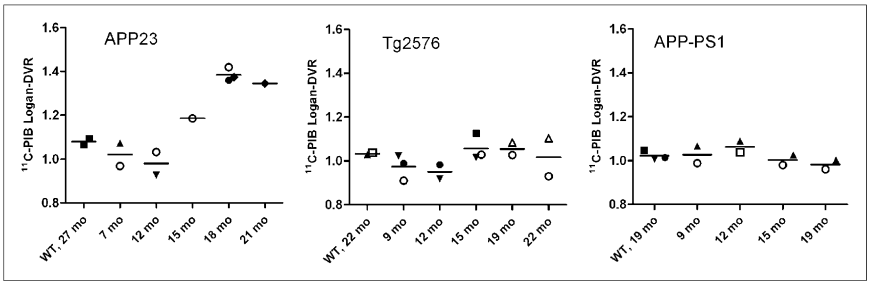


FIGURE 3. Dynamic PET data were quantitated using Logan graphical method with cerebellar input to obtain DVRs for frontal cortex of APP23, Tg2576, and APP_{swe}-$PS1_{dE9}$ mice. Same symbol is used for individual mice followed longitudinally in various time points. WT = wild-type.

Downloaded from jnm.snmjournals.org by on March 15, 2017. For personal use only.

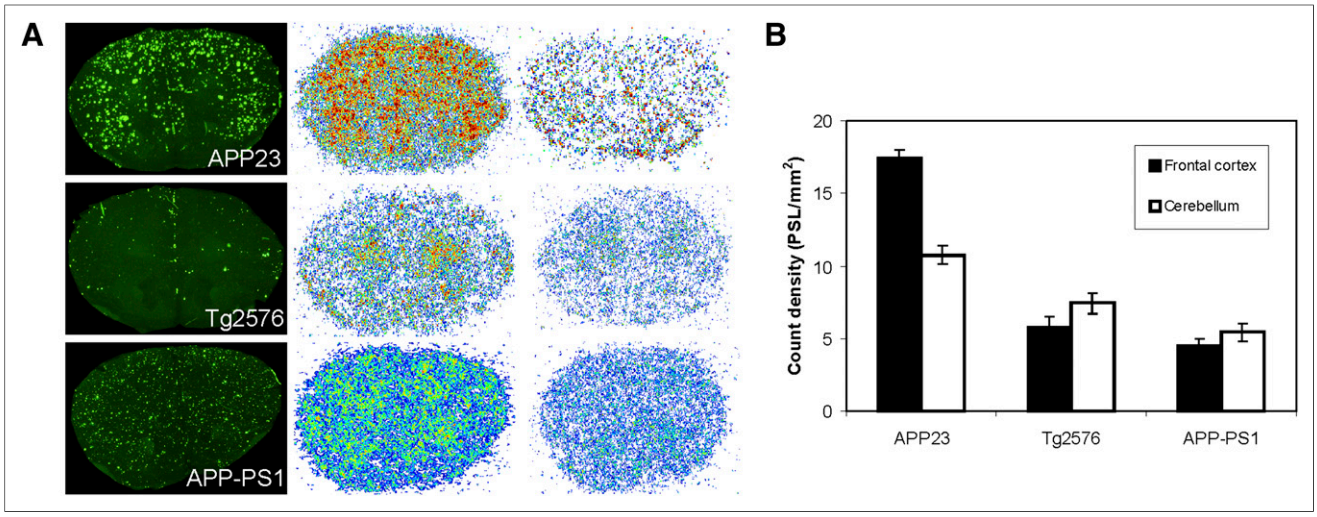


FIGURE 4. (A) Thioflavin-S staining and ex vivo ^{11}C-PIB autoradiograms from frontal cortex (FC) of APP23, Tg2576, and APP_{swe}-$PS1_{dE9}$ mice and ex vivo ^{11}C-PIB autoradiograms of wild-type control mice. (B) Count densities for FC and cerebellum (CB) for APP23, Tg2576, and APP_{swe}-$PS1_{dE9}$ mice. Data are expressed as mean count density (photostimulated luminescence per unit square millimeter) ± SD.

brain, but they were small and stained less intensely than in APP23 or Tg2576 mice. In contrast to APP23 and Tg2576 mice, thioflavin-S–positive deposits were also detected in the CB of APP_{swe}-$PS1_{dE9}$ mice (Supplemental Fig. 3). Only APP23 mice exhibited clear increases in Logan DVRs as the fibrillar Aβ burden in the brain increased (Fig. 5B).

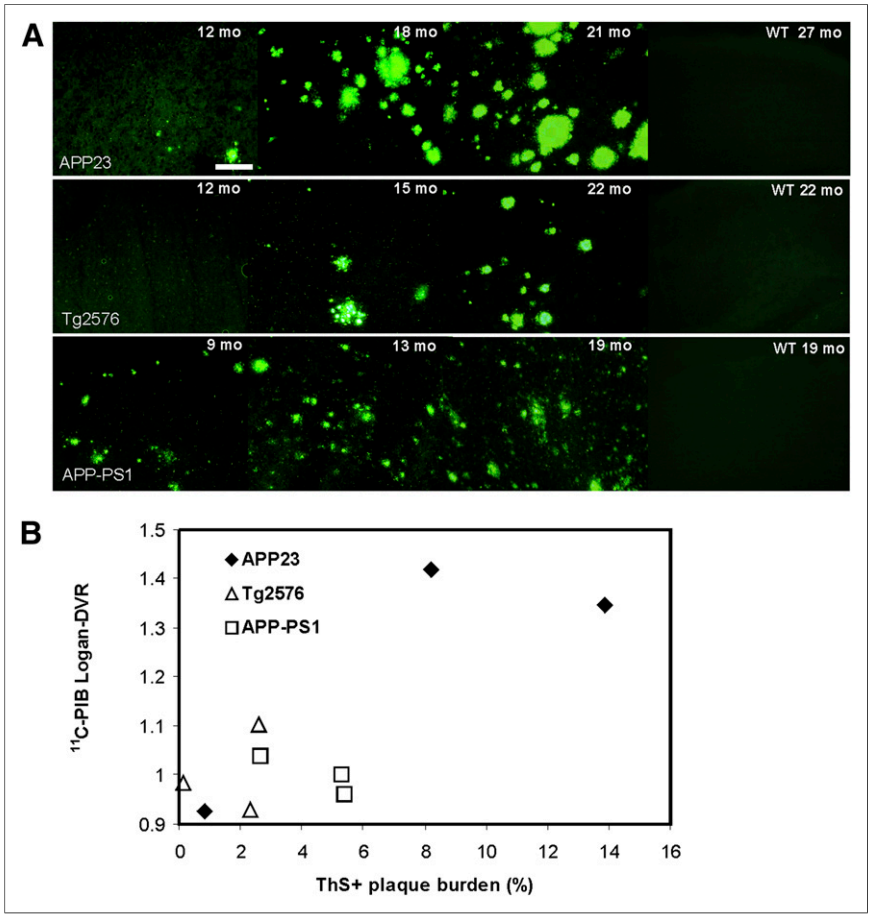


FIGURE 5. (A) Thioflavin-S staining of cortical sections from APP23, Tg2576, APP_{swe}-$PS1_{dE9}$, and wild-type (WT) control mouse brain at various ages. (B) Relationship between thioflavin-S–positive Aβ deposition and DVRs obtained from in vivo PET scans for individual APP23, Tg2576, and APP_{swe}-$PS1_{dE9}$ mice. Scale bar = 200 μm.

Representative cortical images of $Aβ_{1–40}$-immunoreactive deposits are presented in Figure 6A. APP23 mice showed only sparse $Aβ_{1–40}$-immunoreactive deposits at 12 mo of age, but in parallel with the increasing thioflavin-S staining, extensive numbers of large, dense-cored plaques were observed at 18 and 21 mo in cortical regions. Tg2576 mice first exhibited sparse $Aβ_{1–40}$-positive deposits at 15 mo of age; even at 22 mo, the deposits were small in amount and size. APP_{swe}-$PS1_{dE9}$ mice exhibited extensive $Aβ_{1–40}$ immunostaining throughout the cortex already at 9 mo. The plaque load increased slightly as the mice aged, and abundant $Aβ_{1–40}$ immunostaining was detected throughout the brain and in the CB at 19 mo. In APP23 mice only, ^{11}C-PIB binding quantitated as Logan DVRs increased in parallel with the $Aβ_{1–40}$-stained plaque load (Fig. 6B).

Representative cortical images of thioflavin-S and 6E10-immunoreactive deposits are presented in Figure 7. In the cortex of APP23 mice, most 6E10 staining was colocalized with fibrillar deposits. In the hippocampus, fewer thioflavin-S–positive deposits were seen, and 6E10 staining dominated. In the Tg2576 brain, 6E10 staining was more abundant than fibrillar Aβ staining with thioflavin-S. Overall, APP_{swe}-$PS1_{dE9}$ mice exhibited the highest Aβ deposition in the brain at all evaluated ages measured by 6E10 staining, and thioflavin-S/6E10–stained deposits were highly colocalized.

Downloaded from jnm.snmjournals.org by on March 15, 2017. For personal use only.

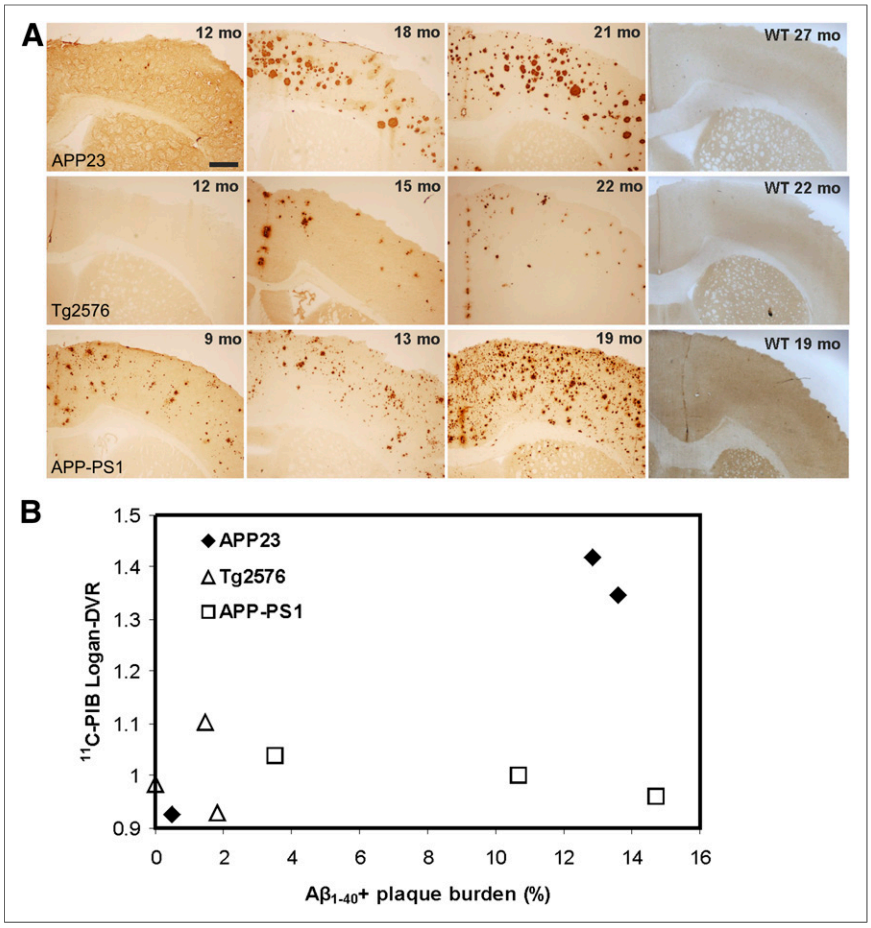


FIGURE 6. (A) $A\beta_{1-40}$-immunoreactive Aβ deposits in cortical sections of APP23, Tg2576, APP_{swe}-$PS1_{dE9}$, and wild-type control mouse brain at various ages. (B) Relationship between anti-$A\beta_{1-40}$-immunoreactive plaque deposition and DVRs obtained from in vivo PET scans. Scale bar = 500 μm.

Large, $A\beta_{N3pE}$-immunoreactive deposits were detected in the NC of APP23 mice at 18 and 21 mo. No $A\beta_{N3(pE)}$-immunoreactive deposits were detected in Tg2576 or APP_{swe}-$PS1_{dE9}$ mice (Supplemental Fig. 4).

DISCUSSION

The present study demonstrated that moderate SA ^{11}C-PIB and small-animal PET imaging can be used to longitudinally follow the accumulation of Aβ deposits in the brain of APP23, but not in Tg2576 or APP_{swe}-$PS1_{dE9}$, transgenic mice despite the increasing Aβ deposition in the brain. The results show that ^{11}C-PIB imaging can be used to investigate the effect of antiamyloid therapies in the same mice longitudinally and, possibly, combined with behavioral testing, also enable clinical correlations. Furthermore, new antiamyloid therapies are still being developed and may benefit from feasible in vivo models of efficacy on brain Aβ load.

A previous study reported successful follow-up of Aβ accumulation with in vivo PET in APP23 mice; however, that study used ^{11}C-PIB produced with a very high SA (290 ± 10 GBq/μmol at the end of synthesis), and thus a similar approach is not feasible in most imaging centers (*11*). In the present study, we report that brain retention of ^{11}C-PIB shows a clear increase in aging APP23 mice even with an SA of 100 ± 27 GBq/μmol at the end of synthesis, indicating the high importance of the used mouse model for ^{11}C-PIB–positive results.

Significant differences in the FC/CB radioactivity ratios between 22-mo-old Tg2576 transgenic mice and their wild-type control mice have been observed previously with ^{11}C-PIB (*9*). However, the differences were small, and the authors concluded that the specific binding of ^{11}C-PIB to Aβ was low in Tg2576 mice. In the present study, we failed to detect any increase in Logan DVRs or B/F_{40-60} ratios in aging Tg2576 mice, or any difference between wild-type and transgenic mice, even during the final evaluation at 22 mo of age. In the Tg2576 mice used in this study, few Aβ deposits were present even at 22 mo. However, we believe that longer follow-up times are impractical, as working with mice as old as 22 mo already involves practical problems with animal survival.

Weak binding of ^{11}C-PIB to brain Aβ has also been observed previously in APP-PS1 double-transgenic mice (*10*). At 12 mo, when the Aβ deposition in these mice already exceeds the relative deposition observed in the human AD brain, no significant ^{11}C-PIB retention was observed in the mouse brain in vivo (*10*). These results were verified with ex vivo autoradiography and in vitro binding studies, which revealed less than one high-affinity binding site per 1,000 Aβ molecules (*10*). However, there are many different double-transgenic mouse models expressing APP and PS1 mutations (referred to in the literature as APP-PS1 mice), and differences in plaque morphology are to be expected (*6,12,21,22*). In a more recent study, Manook et al. used small-animal PET imaging and ^{11}C-PIB to successfully differentiate transgenic APP-PS1 mice (B6;CB-Tg(Thy1-PSEN1*M146V/Thy1-APP*swe)-10Arte, TaconicArtemis GmbH) from wild-type control mice. Different transgenic groups could also be differentiated by the levels of ongoing Aβ pathology in the brain (*12*). However, in the double-transgenic APP_{swe}-$PS1_{dE9}$ model used in our study, the imaging results resembled those of wild-type control mice and were similar to the earlier findings of Klunk et al., obtained with mice with APP_{swe} and M146 L PS1 mutations (*10*).

We observed clear differences in the appearance, structure, and amount of Aβ deposits between the evaluated transgenic mouse models. Numerous lines of transgenic mice are available for AD research, and many variables, including the number and choice of transgenes, the used promoters, the background strain, and the sex of the animals, affect the pathology expressed by different mouse lines (*6*). Unsurprisingly, the structures of Aβ deposits also vary markedly. Slowly forming large, compact Aβ deposits that share many characteristics of human AD deposits exist throughout the APP23 cerebral cortex. An increase in ^{11}C-PIB retention was observed as the cortical plaque load increased in the APP23 animals. Tg2576 mice reportedly exhibit increased Aβ load, classic

Downloaded from jnm.snmjournals.org by on March 15, 2017. For personal use only.

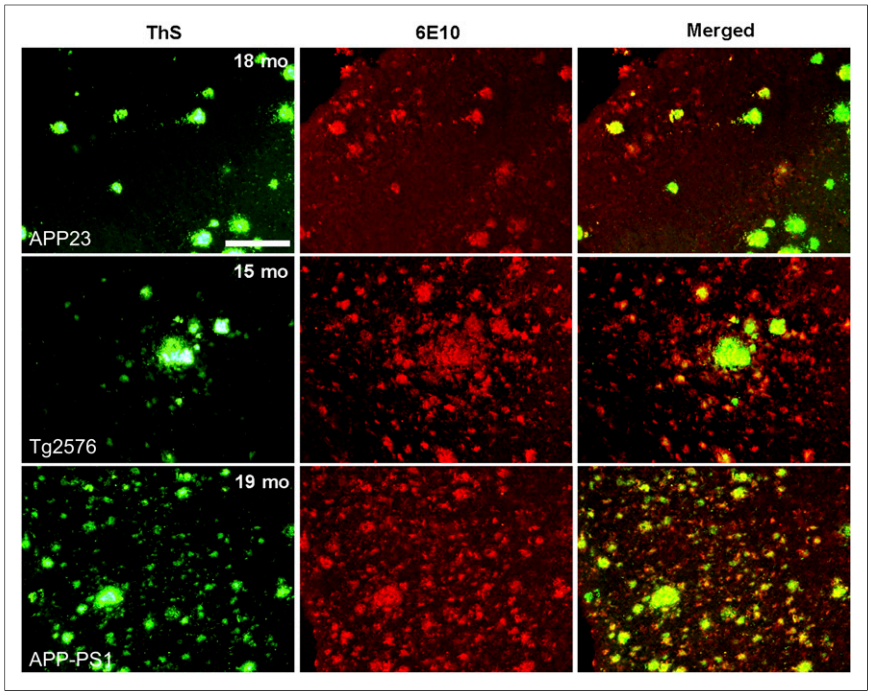


FIGURE 7. Colocalization (yellow) of thioflavin-S–positive Aβ deposits (green) and 6E10 immunoreactive deposits (red) in APP23, Tg2576, and APP_{swe}-$PS1_{dE9}$ brain. Scale bar = 200 μm.

senile plaques, and fibrillar deposits already at 9 mo (*16*). However, in the present study, sparse fibrillar deposition became visible only at 15 mo, and even though these dense-cored deposits were detected with thioflavin-S, their staining intensity was much weaker than that observed in APP23 brains. Overall, development of Aβ deposits in these mice was surprisingly slow and modest and therefore appears impractical for amyloid imaging studies. In APP_{swe}-$PS1_{dE9}$ mice, very high Aβ deposition was visible already at 9 mo immunohistochemically. Although deposition was fast, the Aβ deposition was more diffuse than fibrillar Aβ. In double-transgenic mice with mutations in both APP and PS1, the deletion of PS1 exon 9 reportedly results in PS1 gain of function and the occurrence of large, homogeneous plaques that are only slightly congophilic (*22*). Because the APP_{swe}-$PS1_{dE9}$ mice used in this study contain the same mutations, the presence of Aβ plaques resembling these "cotton wool plaques" is unsurprising. Severe Aβ deposition was also observed in the CB at 19 mo, a finding that does not support the use of this model for cerebellar reference region–based analysis. The calculated FC/pons and FC/CB ratios were, however, virtually identical; this finding indicates that the result is explained by the low binding of ^{11}C-PIB, rather than being an effect of the increased Aβ load in the reference tissue. This is supported by the finding of no ^{11}C-PIB uptake in the CB at 19 mo (Fig. 1C).

The location of PIB binding sites on Aβ deposits is not known at atomic resolution, and multiple binding sites to Aβ fibrils for thioflavin-T and ^{11}C-PIB with different stoichiometries have been proposed (*23,24*). Thus, it is not surprising to observe differences in ^{11}C-PIB binding to Aβ deposits between different mouse lines with different Aβ plaque structure. N-terminally truncated and pyroglutamated forms of Aβ have also been suggested to have a role in ^{11}C-PIB binding (*11*). Because of the suggested binding of thioflavin-T to diverse fibril forms, it has been postulated that $Aβ_{N3(pE)}$ might act as a seeder of fibrillar aggregates, rather than providing ^{11}C-PIB binding sites (*11*). We agree that the same reasons previously proposed to explain the differences in ^{11}C-PIB binding to human and mouse Aβ deposits, including possible posttranslational modifications and different secondary fibrillar structures, might explain the differences in tracer binding to Aβ deposits between different mouse models (*11*).

The number of animals was intentionally kept small because of the longitudinal design of this imaging study, and only 1−4 mice were imaged at each time point. Although the animals were few, the increase in ^{11}C-PIB binding in the aging APP23 brain was clearly detected in individual mice. Additionally, grouping of all the measurements of young (9−12 mo) and old (15−22 mo) transgenic animals revealed increases in $B/F_{40–60}$ ratios in APP23 mice, even with the small number of animals. The results can be considered reliable, as the imaging protocol was the same and each mouse acted as its own control; this is a great advantage of in vivo PET, especially when repeated imaging is performed on precious and very old transgenic animals.

CONCLUSION

In this study, we have shown that in vivo imaging with the amyloid PET tracer ^{11}C-PIB is able to demonstrate brain Aβ deposition in transgenic APP23 mice even if it fails to do the same in the Tg2576 and APP_{swe}-$PS1_{dE9}$ mouse models of AD. Aβ plaque structure and deposition is different in different animal models of AD; careful consideration of the model and the study question is therefore required before PET imaging studies are performed with ^{11}C-PIB or other PET tracers.

DISCLOSURE

The costs of publication of this article were defrayed in part by the payment of page charges. Therefore, and solely to indicate this fact, this article is hereby marked "advertisement" in accordance with 18 USC section 1734. This work was supported by clinical grants from Turku University Hospital (project 13464), the Academy of Finland (project 17652), the Sigrid Jusélius Foundation, and the European Community's Seventh Framework Program (FP7/2007-2013) under grant agreement 212043. The APP23 mice were used with the permission of Novartis Pharma, Switzerland. No other potential conflict of interest relevant to this article was reported.

ACKNOWLEDGMENTS

We thank the staff of the Accelerator Laboratory for radionuclide production, the technical staff of the Radiopharmaceutical Chemistry Laboratory for radiotracer analyses, the staff of MediCity research laboratory for assistance with the animal experiments, and Vesa Oikonen for modeling expertise.

Downloaded from jnm.snmjournals.org by on March 15, 2017. For personal use only.

REFERENCES

1. Nordberg A, Rinne JO, Kadir A, Långström B. The use of PET in Alzheimer disease. *Nat Rev Neurol.* 2010;6:78–87.
2. Rinne JO, Brooks DJ, Rossor MN, et al. ^{11}C-PiB PET assessment of change in fibrillar amyloid-beta load in patients with Alzheimer's disease treated with bapineuzumab: a phase 2, double-blind, placebo-controlled, ascending-dose study. *Lancet Neurol.* 2010;9:363–372.
3. Klunk WE, Engler H, Nordberg A, et al. Imaging brain amyloid in Alzheimer's disease with Pittsburgh Compound-B. *Ann Neurol.* 2004;55:306–319.
4. Klunk WE, Wang Y, Huang GF, et al. The binding of 2-(4′-methylaminophenyl) benzothiazole to postmortem brain homogenates is dominated by the amyloid component. *J Neurosci.* 2003;23:2086–2092.
5. Mathis CA, Wang Y, Holt DP, Huang GF, Debnath ML, Klunk WE. Synthesis and evaluation of ^{11}C-labeled 6-substituted 2-arylbenzothiazoles as amyloid imaging agents. *J Med Chem.* 2003;46:2740–2754.
6. Duyckaerts C, Potier MC, Delatour B. Alzheimer disease models and human neuropathology: similarities and differences. *Acta Neuropathol.* 2008;115:5–38.
7. Dodart JC, Mathis C, Bales KR, Paul SM. Does my mouse have Alzheimer's disease? *Genes Brain Behav.* 2002;1:142–155.
8. Ashe KH, Zahs KR. Probing the biology of Alzheimer's disease in mice. *Neuron.* 2010;66:631–645.
9. Toyama H, Ye D, Ichise M, et al. PET imaging of brain with the beta-amyloid probe, [^{11}C]6-OH-BTA-1, in a transgenic mouse model of Alzheimer's disease. *Eur J Nucl Med Mol Imaging.* 2005;32:593–600.
10. Klunk WE, Lopresti BJ, Ikonomovic MD, et al. Binding of the positron emission tomography tracer Pittsburgh compound-B reflects the amount of amyloid-beta in Alzheimer's disease brain but not in transgenic mouse brain. *J Neurosci.* 2005;25:10598–10606.
11. Maeda J, Ji B, Irie T, et al. Longitudinal, quantitative assessment of amyloid, neuroinflammation, and anti-amyloid treatment in a living mouse model of Alzheimer's disease enabled by positron emission tomography. *J Neurosci.* 2007;27:10957–10968.
12. Manook A, Yousefi BH, Willuweit A, et al. Small-animal PET imaging of amyloid-beta plaques with [^{11}C]PiB and its multi-modal validation in an APP/PS1 mouse model of Alzheimer's disease. *PLoS ONE.* 2012;7:e31310.
13. Kemppainen NM, Aalto S, Wilson IA, et al. Voxel-based analysis of PET amyloid ligand [^{11}C]PIB uptake in Alzheimer disease. *Neurology.* 2006;67:1575–1580.
14. Sturchler-Pierrat C, Abramowski D, Duke M, et al. Two amyloid precursor protein transgenic mouse models with Alzheimer disease-like pathology. *Proc Natl Acad Sci USA.* 1997;94:13287–13292.
15. Calhoun ME, Wiederhold KH, Abramowski D, et al. Neuron loss in APP transgenic mice. *Nature.* 1998;395:755–756.
16. Hsiao K, Chapman P, Nilsen S, et al. Correlative memory deficits, Abeta elevation, and amyloid plaques in transgenic mice. *Science.* 1996;274:99–102.
17. Jankowsky JL, Fadale DJ, Anderson J, et al. Mutant presenilins specifically elevate the levels of the 42 residue beta-amyloid peptide in vivo: evidence for augmentation of a 42-specific gamma secretase. *Hum Mol Genet.* 2004;13:159–170.
18. Franklin KBJ, Paxinos G. *The Mouse Brain in Stereotactic Coordinates.* 3rd ed. Waltham, Massachusetts: Academic Press; 2008.
19. Logan J, Fowler JS, Volkow ND, Wang GJ, Ding YS, Alexoff DL. Distribution volume ratios without blood sampling from graphical analysis of PET data. *J Cereb Blood Flow Metab.* 1996;16:834–840.
20. Snellman A, Rokka J, Lopez-Picon FR, et al. Pharmacokinetics of [^{18}F]flutemetamol in wild-type rodents and its binding to beta amyloid deposits in a mouse model of Alzheimer's disease. *Eur J Nucl Med Mol Imaging.* 2012;39:1784–1795.
21. Bacskai BJ, Hickey GA, Skoch J, et al. Four-dimensional multiphoton imaging of brain entry, amyloid binding, and clearance of an amyloid-beta ligand in transgenic mice. *Proc Natl Acad Sci USA.* 2003;100:12462–12467.
22. Garcia-Alloza M, Robbins EM, Zhang-Nunes SX, et al. Characterization of amyloid deposition in the APPswe/PS1dE9 mouse model of Alzheimer disease. *Neurobiol Dis.* 2006;24:516–524.
23. Lockhart A, Ye L, Judd DB, et al. Evidence for the presence of three distinct binding sites for the thioflavin T class of Alzheimer's disease PET imaging agents on beta-amyloid peptide fibrils. *J Biol Chem.* 2005;280:7677–7684.
24. Wu C, Bowers MT, Shea JE. On the origin of the stronger binding of PIB over thioflavin T to protofibrils of the Alzheimer amyloid-β peptide: a molecular dynamics study. *Biophys J.* 2011;100:1316–1324.

Downloaded from jnm.snmjournals.org by on March 15, 2017. For personal use only.

JNM The Journal of NUCLEAR MEDICINE

Longitudinal Amyloid Imaging in Mouse Brain with ^{11}C-PIB: Comparison of APP23, Tg2576, and APP $_{swe}$-PS1$_{dE9}$ Mouse Models of Alzheimer Disease

Anniina Snellman, Francisco R. López-Picón, Johanna Rokka, Mario Salmona, Gianluigi Forloni, Mika Scheinin, Olof Solin, Juha O. Rinne and Merja Haaparanta-Solin

J Nucl Med. 2013;54:1434-1441.
Published online: July 5, 2013.
Doi: 10.2967/jnumed.112.110163

This article and updated information are available at:
http://jnm.snmjournals.org/content/54/8/1434

Information about reproducing figures, tables, or other portions of this article can be found online at:
http://jnm.snmjournals.org/site/misc/permission.xhtml

Information about subscriptions to JNM can be found at:
http://jnm.snmjournals.org/site/subscriptions/online.xhtml

The Journal of Nuclear Medicine is published monthly.
SNMMI | Society of Nuclear Medicine and Molecular Imaging
1850 Samuel Morse Drive, Reston, VA 20190.
(Print ISSN: 0161-5505, Online ISSN: 2159-662X)

© Copyright 2013 SNMMI; all rights reserved.

SNMMI SOCIETY OF NUCLEAR MEDICINE AND MOLECULAR IMAGING